PHOTOSYNTHETICA
International Journal for Photosynthesis Research

DOI 10.32615/ps.2023.038 PHOTOSYNTHETICA 62 (1): 27-39, 2024

Heterocapsa cf. *bohaiensis* (dinoflagellate): identification and response to nickel and iron stress revealed through chlorophyll *a* fluorescence

V. MÉRIOT[*,**,+,†], A. ROUSSEL[*,**,†], N. BRUNET[***], N. CHOMERAT[#], G. BILIEN[#], L. LE DÉAN[**], V. BERTEAUX-LECELLIER[##], N. COULOMBIER[###], N. LEBOUVIER[*], and T. JAUFFRAIS[**,+]

ISEA, EA7484, Campus de Nouville, University of New Caledonia, 98851 Nouméa, New Caledonia[*]
Ifremer, IRD, University of New Caledonia, University of La Réunion, CNRS, UMR 9220 ENTROPIE, 101 Promenade Roger Laroque, 98897 Nouméa, New Caledonia[**]
CRESICA, 98851 Nouméa, New Caledonia[***]
Ifremer, Littoral – LERBO, Place de la Croix, Concarneau, F-29900, France[#]
CNRS, Ifremer, IRD, University of New Caledonia, University of La Réunion, UMR 9220 ENTROPIE, 101 Promenade Roger Laroque, Nouméa, New Caledonia[##]
ADECAL Technopole, 1 Bis Rue Berthelot, 98846 Nouméa, New Caledonia[###]

Abstract

Metal toxicity in marine ecosystems is a growing issue owing to terrestrial runoff and anthropogenic pollution. *Heterocapsa* cf. *bohaiensis*, a newly isolated dinoflagellate from New Caledonia, was cultivated in photobioreactors operating continuously with high concentrations (10^{-3} M) of nickel (Ni^{2+}) and/or iron (Fe^{2+}) and their photosynthetic efficiency was assessed. The photosynthetic measurements indicated that *H.* cf. *bohaiensis* was tolerant to Ni^{2+} but sensitive to Fe^{2+} high concentrations. In the presence of Fe^{2+}, maximum quantum efficiency and maximal relative electron transport rate decreased from 0.62 to 0.47 and from 156 to 102, respectively. The JIP-tests suggested a reduction of the photosynthesis in response to Fe^{2+} due to a disruption in the electron transport chain rather than a defect in the light absorption and trapping capacity which were on the contrary enhanced by Fe^{2+}. These results bring new knowledge on the impact of nickel and iron on microalgae photosynthetic pathways.

Keywords: dinoflagellate; metal stress; metallic trace elements; microalgae; PAM fluorometry; photosynthesis.

Introduction

High metal concentrations in aquatic ecosystems is a worldwide preoccupying topic since metals accumulate in the trophic chain to ultimately contaminate human through food-chain transfers (Seco *et al.* 2021). New Caledonia is a tropical island located in the Southwest Pacific with coastal waters enriched in trace metals (Ambatsian *et al.*

Highlights

- We found a tolerance of *Heterocapsa* cf. *bohaiensis* to high concentrations of Ni^{2+}
- Absorption, dissipation, and trapping specific fluxes increased in response to high concentrations of Fe^{2+}
- Fe^{2+} induced a decrease in quantum efficiency parameters (F_v/F_m, rETRm), probably due to a disruption of the electron transport chain

Received 27 July 2023
Accepted 12 October 2023
Published online 2 January 2024

[+]Corresponding authors
e-mail: vincent.meriot95@hotmail.com
thierry.jauffrais@ifremer.fr

Abbreviations: BI – Bayesian inference; Fd – ferredoxin; ITS – internal transcribed spacer; M_0 – slope at the origin of fluorescence rise (O–J); ML – Maximum likelihood; PAM – Pulse Amplitude Modulated; PBR – photobioreactor; PC – plastocyanin; PCR – polymerase chain reaction; PQ – plastoquinone; RC – reaction center; rDNA – ribosomal deoxyribonucleic acid; RLC – rapid light curves; ROS – reactive oxygen species.

Acknowledgments: The authors acknowledge Ifremer for supporting the Maorix project, Cresica for supporting the MICROCOMET project, and the South Province of New Caledonia for financing the PhD fellowship of V. Meriot and for delivering the sampling authorization (20274-2019/2-ISP/DENV). We would like to thank Adecal Technopole for its technical support.

[†]These authors contributed equally.

Conflict of interest: The authors declare that they have no conflict of interest.

1997, Le Grand *et al.* 2013). Indeed, one-third of the main land surface is covered by ultramafic substrates rich in nickel, iron, chrome, cobalt, and manganese trace metals but poor in nitrogen, phosphorus, and potassium (Pelletier 2007, Merrot 2019). These metals are naturally present in coastal ecosystems due to leaching and natural erosion *via* ultramafic catchments (Bird *et al.* 1984, Biscéré *et al.* 2017, Merrot *et al.* 2022). However, owing to anthropic activities such as urbanisation and particularly mining operation, metal concentrations have increased over the last decades due to large amounts of terrestrial discharge in the coastal ecosystems (Biscéré *et al.* 2015, Merrot *et al.* 2022). Microalgae living in nickel (Ni) and iron-rich (Fe) coastal waters of New Caledonia are models of choice to study physiological responses to metal stresses. *Heterocapsa* cf. *bohaiensis*, a recently described dinoflagellate species with haemolytic activity (Zhang *et al.* 2019), has been associated with shrimp (*Penaeus japonicus*) and crab (*Eriocheir sinensis*) mortalities in culture in a coastal area of the Liaoning province in China (Xiao *et al.* 2018). This species has been isolated in New Caledonian coastal waters where blue shrimp (*Penaeus stylirostris*) production is the leading aquaculture sector, which raised new risk for the New Caledonian aquaculture industry. In addition, dinoflagellates are known to form harmful algal blooms and produce metabolites of interest and toxins. Moreover, it is admitted that the *Heterocapsa* genus is highly tolerant to metallic trace elements (Satoh *et al.* 2005) and transfer trace metal elements to bivalves, leading to an accumulation in the food chain (Hédouin *et al.* 2010).

Microalgae are primary producers of marine coastal ecosystems and are therefore the first organisms of the food chain impacted by trace metals in seawater. At low concentrations, metals are essential micronutrients for microalgae (Quigg 2016). For example, Fe is a transition metal recognised as an essential micronutrient for microalgae participating in energy entry and electron transport in photosynthesis as part of photosystems, cytochrome b_6f, and Fe-S complexes (Fox and Zimba 2018). Ni is an essential micronutrient necessary for the activity of several enzymes such as the urease, a key enzyme in N-metabolism (Quigg 2016). However, at high concentrations, Ni and Fe may be toxic to microalgae (Wan *et al.* 2014, Martínez-Ruiz and Martínez-Jerónimo 2015, Dahmen-Ben Moussa *et al.* 2018, Yong *et al.* 2019, Guo *et al.* 2022). At high concentrations, most metallic trace elements induce oxidative stress due to the production of reactive oxygen species (ROS) that damage lipidic membranes and cytoplasmic proteins (Danouche *et al.* 2022). Boisvert *et al.* (2007) observed a significant decline of the F_v/F_m and chlorophyll *a* fluorescent transients following Ni^{2+} [mmol mg^{-1}(Chl)] exposure on PSII submembrane fraction isolated from spinach. When *Phaeodactylum tricornutum* was exposed to 5.59 µg(Fe^{2+}) L^{-1}, the F_v/F_m increased, the rETR parameters [the initial rapid light curve slope (α), the light-saturating index (Ek), and the maximum relative electron transport rate (rETRm)] were higher compared to the control condition Fe^{2+}-depleted (Wang *et al.* 2023). As a result, physiological parameters such as growth, photosynthesis efficiency, and antioxidant activity of microalgae are impacted by trace metals concentration (Martínez-Ruiz and Martínez-Jerónimo 2015, Yong *et al.* 2019, Guo *et al.* 2022).

In parallel, microalgae metabolites are highly valuable compounds for cosmetic, pharmaceutical, and agro-alimentary products (Mimouni *et al.* 2012, Chénais 2021). Some microalgae pigments have anti-inflammatory, antibacterial, anticancer, anti-UV, and/or antioxidant properties that might have applications in health care (Sathasivam and Ki 2018). Finally, biotechnologies using microalgae to sequester and remove metals from polluted waters are intensely developed (Leong and Chang 2020). Indeed, some species can absorb high amounts of metal. For example, *Dunaliella* sp. can absorb up to 0.21 pg(Ni) $cell^{-1}$ when exposed to 500 mg(Ni) L^{-1} (Dahmen-Ben Moussa *et al.* 2018). Therefore, understanding trace metal requirements, accumulation, and toxicity for microalgae is critical for their successful cultivation and exploitation in various applications, including metabolites production for biotechnological application and wastewater treatment (Mandal *et al.* 2019, Leong and Chang 2020).

Environmental and culture conditions highly influence microalgae physiology which will affect their growth and photosynthetic efficiency. The PSII efficiency is therefore a good marker of microalgae fitness under abiotic stresses such as metallic trace elements (Coulombier *et al.* 2020, Menguy *et al.* 2020, Wang *et al.* 2023). PAM fluorometry is a commonly used technique to assess PSII efficiency in microalgae (Antal *et al.* 2009) and has the advantage of being reliable, fast, and noninvasive (Schreiber *et al.* 1995). Briefly, in response to light, microalgae either dissipate light energy into heat, emit fluorescence, or use it for photochemistry. By measuring the fluorescence emitted by chlorophyll *a* of PSII, the PAM fluorometer gives information on light dissipation and light use in photochemistry (Consalvey *et al.* 2005).

The objective of the current study was to evaluate, using PAM fluorometry, the effect of high concentrations of Ni^{2+} and Fe^{2+} on *H.* cf. *bohaiensis* growth and photosynthetic efficiency. Experiments were performed in photobioreactors operated continuously to observe short- and long-term effects of the two metals and a mixture of both and to provide adaptive photophysiological traits following the exposure to high metal concentration.

Materials and methods

Sampling sites, isolation, and culture conditions: New Caledonia, located approximately 1,500 km east of Australia in the Southwestern Pacific Ocean, consists of numerous islands, with the main island known as Grande Terre. An ultramafic bedrock (including Isle of Pines totalling ~ 5,470 km^2) covers about one-third of its surface area. The strains of interest (19PV99 and 20PV100) were isolated from the experimental aquaculture station of Saint Vincent (Boulouparis), situated on the west coast of Grande Terre and from Kuto Bay (Isle of Pines), an island situated at the south of Grande Terre.

The first strain (19PV99) was isolated from a bloom, in November 2019, in shrimp earthen pounds (coordinates: 21°55'35.7"S, 166°05'01.4"E), and the second from a bloom, in January 2020, in an enclosed sandy bay (22°39'25.4"S, 167°26'34.4"E). In the laboratory, the samples were diluted in autoclaved seawater enriched in L1 culture medium (Guillard and Hargraves 1993), and a small artificial light device was used to attract the mobile cells and create a small bloom close to the surface of the culture dishes. Small drops were then sampled and transferred into cell culture multi dishes filled with filtered (0.2 µm), autoclaved, and L1 enriched seawater. The strains were subsequently cultured in a thermo-controlled incubator at 27°C, under illumination of 50 µmol(photon) m^{-2} s^{-1} with a 16/8-h light/dark photoperiod. Finally, the strains (19PV99 and 20PV100) were transferred to 150-mL Erlenmeyer flasks containing 50 mL of L1-enriched seawater and maintained in our culture collection under similar conditions.

DNA amplification and sequencing: The cultures were extracted with the *PCRBIO Rapid Extract PCR* Kit (*PCR Biosystems Ltd.*) which combines extraction and polymerase chain reaction (PCR). In a 1.5-mL tube, 1 mL of culture was taken and centrifuged for 3 min at 14,000 rpm. The supernatant was discarded to retain only the pellet. Then the manufacturer's instructions were followed, except for the step dilution where 190 µL of PCR-grade dH_2O were added instead of 900 µL. A nested PCR was used to amplify the ribosomal deoxyribonucleic acid (rDNA) gene combined with small partial (SSU) and large subunit ribosomal including the internal transcribed spacer (ITS). The first round of PCR used SR9-FW (Freeman *et al.* 2004) and D3B (Nunn *et al.* 1996) primers. Two-second rounds of PCR were carried out separately using 1 µL of the amplicon previously obtained with primers SR9FW and D2C (Scholin *et al.* 1994) or D1R (Scholin *et al.* 1994) and D3B. The PCR reaction was performed using a *PCR Master Mix Promega* kit following the manufacturer's instructions. Amplicons obtained were visualized on a 1% agarose gel after electrophoresis and the positive samples were purified using the *ExoSAP-IT PCR Product Cleanup* reagent (*Affymetrix*, Cleveland, OH, USA) and sequenced (*Big Dye Terminator v. 3.1 Cycle Sequencing Kit*; *Applied Biosystems*, Tokyo, Japan). Primers and excess dye-labelled nucleotides were first removed using the *Big Dye X-Terminator Purification* kit (*Applied Biosystems*, Foster City, CA, USA). Sequencing products were run on an *ABI PRISM 3130* Genetic Analyzer (*Applied Biosystems*).

Phylogenetic analysis: For both strains (19PV99 and 20PV100), sequences including partial 18S rDNA (OR194073, OR224571), ITS region (OR194143, OR224570), and partial 28S rDNA (OR194153, OR224569) were obtained. They were used in a phylogenetic analysis inferred from a concatenated matrix including partial 18S rDNA, internal transcribed spacer 1, 5.8S rDNA, internal transcribed spacer 2, and partial 28S rDNA of various *Heterocapsa* species and *Prorocentrum*/*Azadinium* as outgroup. Each region was separately aligned using the *MAFFT* algorithm with the *q-ins-i* option (Katoh *et al.* 2019). Alignments were then concatenated using *SeaView* software (Gouy *et al.* 2010). The final alignment matrix comprised 93 sequences and 4,006 characters including gaps (1,745 characters for 18S, 194 characters for 5.8S, and 877 characters for 28S). A list of all sequences included and accession numbers is given in Table 1S (*supplement*). Phylogenetic trees were calculated with Bayesian inference (BI) and Maximum likelihood (ML). The model used for the calculations was selected using *jModelTest v. 2* (Darriba *et al.* 2012) and the *General Time Reversible* model with 4 gamma rate categories, was found to be the most appropriate for the dataset and was chosen for phylogenetic analysis.

ML phylogenetic trees were generated using *PHY-ML v. 3.3* (Guindon *et al.* 2010) with 1,000 bootstraps. BI was performed to estimate Posterior Probability distribution using *MrBayes 3.2.6* with *Metropolis-Coupled Markov chain Monte Carlo* simulations (Ronquist and Huelsenbeck 2003). Trees were sampled every 100 generations for 4,000,000 generations and the first 400,000 generations were discarded as burn-in. Phylogenies were visualized using *SeaView* and *Inkskape* software. Genetic *p*-distances were calculated using *Mega software v. 11.0.13* (Tamura *et al.* 2021).

Photobioreactor culture conditions and metal stress: Cultures were carried out in three 10-L stirred closed photobioreactors (PBRs) made of transparent polymethylmethacrylate (Menguy *et al.* 2020). The pH was maintained at 8.2 using automated CO_2 injections and the temperature was kept constant at 26°C by thermal exchange. The light was set at 200 µmol(photon) m^{-2} s^{-1} meter at the center of the PBR using a *LI-COR* quantum sensor and applied continuously. Cultures were homogenized using a Rushton turbine at 92 rpm and aerated by bubbling air filtered at 0.2 µm. Before inoculation, each PBR was sterilized for 20 min with a 5‰ *DEPTIL PA5* and rinsed twice with 0.2 µm filtered seawater. Each PBR was then filled with 9.2 L of enriched seawater (L1 medium) and inoculated with 0.8 L of *H.* cf. *bohaiensis* (strain 20PV100) culture. PBRs were first maintained in batch culture conditions for 5 d. Culture growth and cell vitality were monitored daily using optical density at 680 and 800 nm and by counting and observing cells on a *Malassey* hemocytometer (Coulombier *et al.* 2021). After 5 d in batch, the PBRs were switched to continuous culture mode with a renewal rate of 30% per day until steady state (*i.e.*, less than 10% of optical density and cell concentration variations over 3 d). At steady state, the solution of metals was injected in the PBRs and added to the L1 culture medium to reach a concentration in the PBRs and culture media of 10^{-3} M of Ni^{2+}, 10^{-3} M of Fe^{2+}, and a mixture of Ni^{2+} + Fe^{2+} at 0.5×10^{-3} M each in PBR 1, 2, and 3, respectively. Metals availability in the metal-enriched culture media was evaluated and controlled using *CHEAQS 0.2.1.8*. This experiment was replicated three times.

Photosynthetic parameter measurements: Photosynthetic parameters of *H.* cf. *bohaiensis* were monitored using a PAM fluorometer (*AquaPen-C AP 110-C*, *Photon Systems Instruments*, Czech Republic) equipped with a blue-light emitting diode at 470 nm. All measurements were performed under dark-adapted (15 min) conditions and at steady state before metal exposure (t_0), and after metal exposure during the transient phase at 24 h (t_{24}), and after 13 d of exposure (t_f). First, the maximum quantum efficiencies (F_v/F_m) of PSII were acquired and on different samples, the rapid light curves (RLCs) were constructed using seven steps of increasing actinic light intensity [10, 20, 50, 100, 300, 500; and 1,000 µmol(photon) m^{-2} s^{-1}] of 60 s each. Data were then fitted to the model by Platt *et al.* (1980) to estimate the physiological parameters rETRm, alpha (α), and Ek. RLCs were also used to calculate the Stern–Volmer coefficient (*i.e.*, nonphotochemical quenching induced by the light curve, $NPQ_{induced}$) (Ralph and Gademann 2005). Then, to capture rapid chlorophyll *a* fluorescent transient, OJIP transients were constructed by measuring polyphasic chlorophyll *a* fluorescence over a 2-s saturating light pulse [3,000 µmol(photon) m^{-2} s^{-1}] on another sample. The JIP-test of Strasser and Strasser (1995) was applied to translate experimental data into biophysics parameters (*1*) ABS/RC, TR_0/RC, DI_0/RC, and ET_0/RC that quantified the specific energy fluxes per reaction centre and (*2*) ψ_0, φD_0, φP_0, and φE_0 that quantified the minimal quantum yield of primary photochemistry during the experiment. Methods used in this paper are summarized in Fig. 1S (*supplement*).

The significations of the photosynthetic parameters are presented below in the text table. F', F_m', F_q', and F_q'/F_m' are measured during the rapid light curves. Other parameters are measured in a dark-adapted state (15 min). A reaction centre (RC) is considered open when Q_A is in its oxidative state, conversely RC close up when Q_A is reduced into Q_A^-. Q_A – primary quinone acceptor; Q_B – secondary quinone acceptor; PQ – plastoquinone; PC – plastocyanine; Cyt b_6f – cytochrome b_6f.

Statistical analysis: Every experimental measurement was done in triplicate and the experimental setup was repeated three times. Data in tables are expressed as

Parameter	Definition	Formula	Interpretation
Rapid light curve			
F_0	Minimum fluorescence after a dark adaptation		Minimum fluorescence when all RC are open
F_m	Maximal fluorescence during a saturating flash		Maximal fluorescence when all RC are closed
F_v	Variable fluorescence	$F_m - F_0$	
F_v/F_m	The maximal quantum yield of PSII photochemistry	$(F_m - F_0)/F_m$	Maximum light-utilisation efficiency of PSII
F'	Initial fluorescence intensity in a light-adapted state		
F_m'	Maximum fluorescence in a light-adapted state under a saturating flash		
F_q'	Fluorescence quench in actinic light	$F_m' - F'$	
F_q'/F_m'	Light-utilisation efficiency	$(F_m' - F')/F_m'$	
rETR	Relative electron transport rate	$(F_q'/F_m') \times PAR \times 0.5$	Ralph and Gademann (2005)
rETR(i)	Relative transport rate of electrons *vs.* irradiance (i) in the absence of photoinhibition	$rETR(i) = rETRm \times (1 - e^{(-\alpha \times i/rETRm)})$	Platt *et al.* (1980)
rETRm	Maximum relative electron transport rate		rETR before levelling off at a maximum light-saturated rate
α	Initial RLC slope, maximum light use coefficient for PSII		Ability to use low light intensities
Ek	Light saturating index [µmol(photon) m^{-2} s^{-1}]	$Ek = rETRm/\alpha$	Ability to use high light intensities
$NPQ_{induced}$	Nonphotochemical quenching induced during RLC experiment	$(F_m - F_m')/F_m'$	Ability to dissipate energy into heat as a photoprotective mechanism
OJIP			
Specific fluxes			
ABS/RC	Average absorption of photons at the antenna per active RC		The apparent antenna size
TR_0/RC	Trapping flux of exciton per active RC		The rate by which an exciton is trapped in RC resulting in the reduction of Q_A to Q_A^-
ET_0/RC	Electron transport flux per active RC (further than Q_A^-)		The rate by which an electron moves from Q_A^- to Q_B, PQ pool, Cyt b_6f and PC
DI_0/RC	Dissipation flux of photon into heat per active RC		

Quantum efficiency			
M_0	Slope at the origin of fluorescence rise (O–J)		Rate of RC closure corresponding to Q_A reduction
φP_0	Maximum quantum yield of primary photochemistry	TR_0/ABS	The probability that an absorbed photon will be trapped into the PSII
φE_0	Quantum yield for electron transport	ET_0/ABS	Quantum yield of electron transport
ψ_0	ET_0/TR_0		The probability that a trapped photon can move an electron into the transport chain further than Q_A^- in the electron transport chain
φD_0	DI_0/ABS		Quantum yield of energy dissipation
πAbs	Performance index	$[\Upsilon_{RC}/(1-\Upsilon_{RC})] \times [\varphi P_0/1-\varphi P_0] \times [\psi E_0/1-\psi E_0]$	The probability that an electron moves from PSII to PQ pool

mean ± standard error (SE) over the triplicate. Variance homogeneity and normality were tested with *Bartlett* and *Shapiro* tests, respectively. Statistical differences at 95% certainty between experimental conditions and time of analyses were tested using an analysis of variance (*ANOVA*) followed by an LSD test. Otherwise, the tests were performed using the *Kruskal–Wallis* test followed by a *Dunn* test. Statistical analyses were performed using the *RStudio* software (R Core Team 2017). Parameters from JIP-test and F_v/F_m were analysed on metal condition data separately.

Results

Phylogenetic analysis: The ML tree (Fig. 1) showed that the two species of *Heterocapsa* isolated in New Caledonia form fully supported clades. The sequence of strain 19PV99 clustered with a group of sequences including strains CCMP2770, CCMP1734, CCMP1322, and QUCCCM85-88, and was identified as *H. pygmaea*. The sequence of strain 20PV100, the one studied in the present article, was closely related to strain HCBC88 and they were basal to the clade formed by sequences of *H. bohaiensis*. Genetic *p*-distances calculated on ITS region (ITS1-5.8S rDNA-ITS2) between strain 20PV100, *H. bohaiensis* isolates and strain USA29-9 was 2.0–2.5%. Calculated on partial LSU rDNA, the *p*-distance between strain 20PV100 and strain HCBC88 and *H. bohaiensis* isolate 4-2 were 0.9 and 2.1%, respectively (not shown).

Growth: Following metal injection, the absorbance at 680 (Fig. 2S, *supplement*) and 800 nm and cell concentration decreased in the Fe^{2+} conditions, while the other two treatments did not affect culture growth (Fig. 2). Cell concentration decreased from $11.20 \times 10^5 \pm 1.35 \times 10^5$ cell mL^{-1} (t_0) to $6.80 \times 10^5 \pm 0.78 \times 10^5$ cell mL^{-1} in the Fe^{2+} condition, while it remained stable in the other conditions.

Chlorophyll *a* fluorescence: The initial maximum light-utilization efficiency, F_v/F_m, used as a proxy of the efficiency of the PSII light utilization for photochemical conversion was similar in the different PBRs (0.62 ± 0.01). However, following metal injection a small decrease was observed after 24 h of exposure, which was found to be significant after 13 d of Ni^{2+} (0.59 ± 0.01), Fe^{2+} (0.47 ± 0.03), and Ni^{2+}+Fe^{2+} (0.50 ± 0.02) exposure ($p<0.05$, $p<0.01$, and $p<0.001$, respectively) (Fig. 3).

To build the RLCs (Fig. 4), the relative electron transport rate rETR was calculated, using a saturating flash pulse at increasing actinic light intensity. In our experiment, the RLCs presented the typical first phases but did not exhibit photoinhibition in any of the three conditions (Fig. 4).

Regarding the maximum relative electron transport rate (rETRm), used as a proxy of photosynthetic activity, although some small differences were noted between PBRs no significant differences were found between initial values before metal injection (rETR = 171.52 ± 8.28). The rETRm decreased gradually from t_0 to t_f under Fe^{2+} and Ni^{2+}+Fe^{2+} high concentrations, while in the Ni^{2+} condition, it decreased at t_{24} and increased at t_f (Table 1). Indeed, following the Ni^{2+} injection, a significant decrease was observed after 24 h ($p<0.01$) from 181.67 ± 20.91 to 141.42 ± 5.39, while in the other conditions, no significant difference was observed between t_0 and t_{24} (Table 1). However, in the Ni^{2+} condition, no difference was observed between the initial and the final rETRm (166.3 ± 17.48), while the rETRm were significantly lower at the end of the experiment in the Fe^{2+} ($p<0.01$) and Ni^{2+}+Fe^{2+} ($p<0.001$) conditions. This decrease was equal to 35 and 27% of the initial rETRm in the Fe^{2+} and Ni^{2+}+Fe^{2+} conditions, respectively (Table 1).

The maximum light-utilization coefficient, α, used as a proxy of the ability to use low light intensities decreased at t_f in Fe^{2+} and Ni^{2+}+Fe^{2+} conditions, from 0.35 ± 0.01 to 0.27 ± 0.01, and from 0.32 ± 0.02 to 0.28 ± 0.004, respectively, while when exposed to Ni^{2+}, α did not vary significantly (Table 1). In each condition, Ek, the light-saturating coefficient that represents a proxy of the ability to use high light intensities follows a similar trend to the rETRm (Table 1). Ek decreased gradually from t_0 to t_f under Fe^{2+} [446.83 ± 18.42 to 378.29 ± 48.06 µmol(photon) m^{-2} s^{-1}] and Ni^{2+}+Fe^{2+} [538.88 ± 31.15 to 452.62 ± 34.84 µmol(photon) m^{-2} s^{-1}] conditions, while in the Ni^{2+} condition, it decreased at t_{24} and increased at t_f (Table 1). All parameters varied significantly between metal conditions and time of analysis except the NPQ induced by the RLC which did not vary over time.

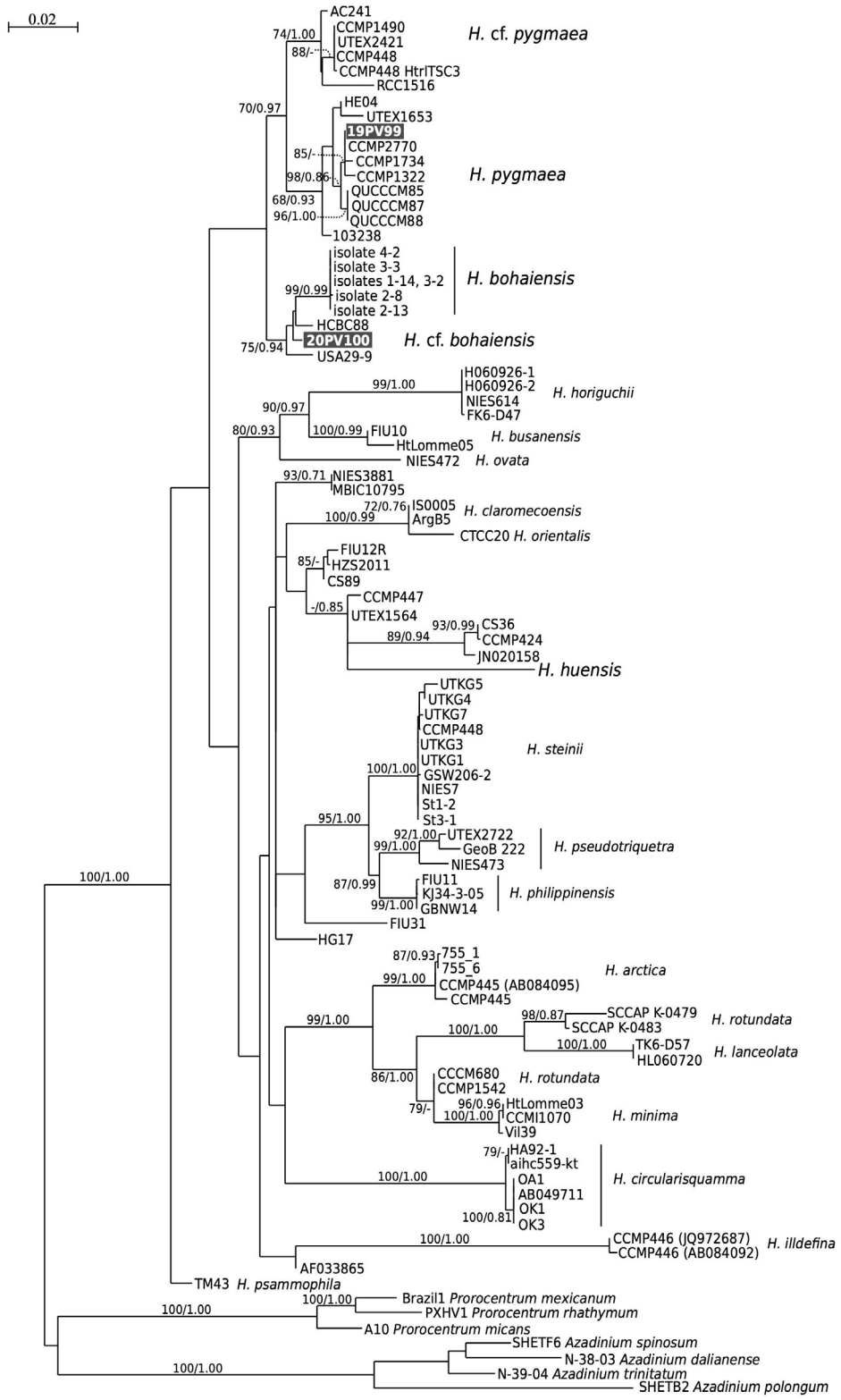

Fig. 1. Maximum likelihood (ML) phylogenetic tree inferred from a concatenated matrix including partial 18S rDNA, internal transcribed spacer 1, 5.8S rDNA, internal transcribed spacer 2, and partial 28S rDNA of various *Heterocapsa* species and *Prorocentrum*/*Azadinium* as outgroup. The strains presented in *boldface on a grey background* are the two *Heterocapsa* isolated in New Caledonia (19PV99 and 20PV100). *Black vertical bars* show distinct *Heterocapsa* clades. Numbers at nodes represent bootstrap support values from ML and posterior probabilities from Bayesian inference (BI). Bootstraps value below 65 and posterior probabilities below 0.70 are indicated with '-'.

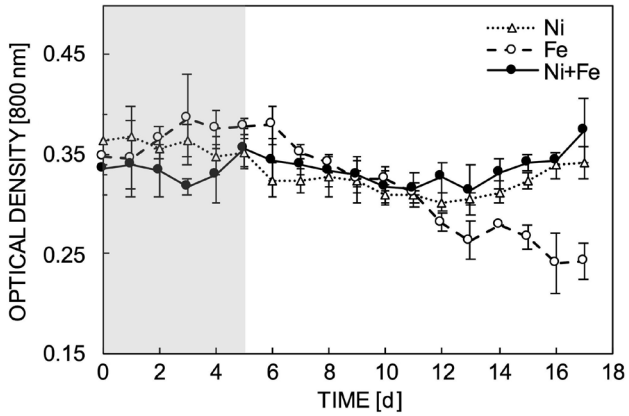

Fig. 2. Culture stability, absorbance at 800 nm of *Heterocapsa* cf. *bohaiensis* cultured in continuous before (*grey part*) and after (*white part*) injection of Ni^{2+}, Fe^{2+}, and Ni^{2+}+Fe^{2+}.

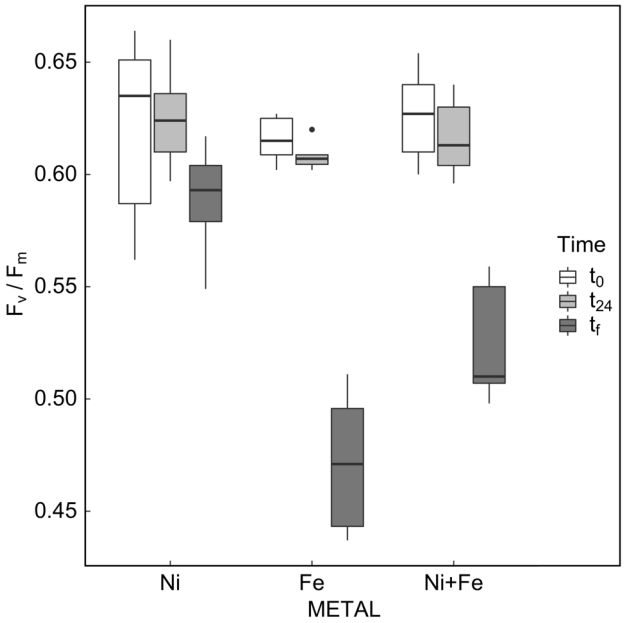

Fig. 3. Boxplot of maximum quantum yields (F_v/F_m) of *Heterocapsa* cf. *bohaiensis* in the presence of Ni^{2+}, Fe^{2+}, or Ni^{2+}+Fe^{2+} high concentrations at t_0, t_{24}, and t_f of the experiment.

Rapid chlorophyll *a* fluorescent transient analysis (JIP-test): In response to a saturating-light pulse, chlorophyll *a* fluorescence exhibits a fast polyphasic rise from an initial fluorescence intensity F_0 (namely O) to a maximal intensity F_m (namely P) and a subsequent decline (Fig. 5*A*,*B*). The slope of the corresponding OJIP transient represents the physiological state of the microalgae (Strasser and Strasser 1995). A reduced slope indicates a slowdown in the electron transport rate. After Ni^{2+} injection, OJIP transients at t_0, t_{24}, and t_f were not different (Fig. 5*D*), while 13 d after Fe^{2+} or Ni^{2+}+Fe^{2+} injections J–I and I–P slopes attributed to the electron transport from Q_A^{2-} to Q_B and finally PSI, decreased compared to t_0 (Fig. 5*B*,*C*).

The photophysiological parameters, F_v/F_m, ABS/RC, TR_0/RC, DI_0/RC, ET_0/RC, ψ_0, φD_0, φP_0, and φE_0 were calculated from OJIP and are provided as a radar plot (Fig. 6). All data of the fluorescence parameters were normalized relative to their respective control (t_0). Ni^{2+} high exposure did not influence significantly any of the previously mentioned parameters. πAbs, the probability that a trapped electron in the RC go further than the plastoquinone pool (PQ) in the electron transport chain, φP_0, the probability that an absorbed electron will be trapped in RC, and φE_0, the quantum yield of electron transport decreased significantly in Fe^{2+} ($p<0.01$) and Ni^{2+}+Fe^{2+} ($p<0.001$; $p<0.01$) conditions after 13 d of exposure (Fig. 6). In addition, in Fe^{2+} and Ni^{2+}+Fe^{2+} conditions, ψ_0, representing the probability that a trapped electron moves further than Q_A decreased ($p<0.05$ for both) at t_f. The slope at the origin of the OJIP transient, M_0,

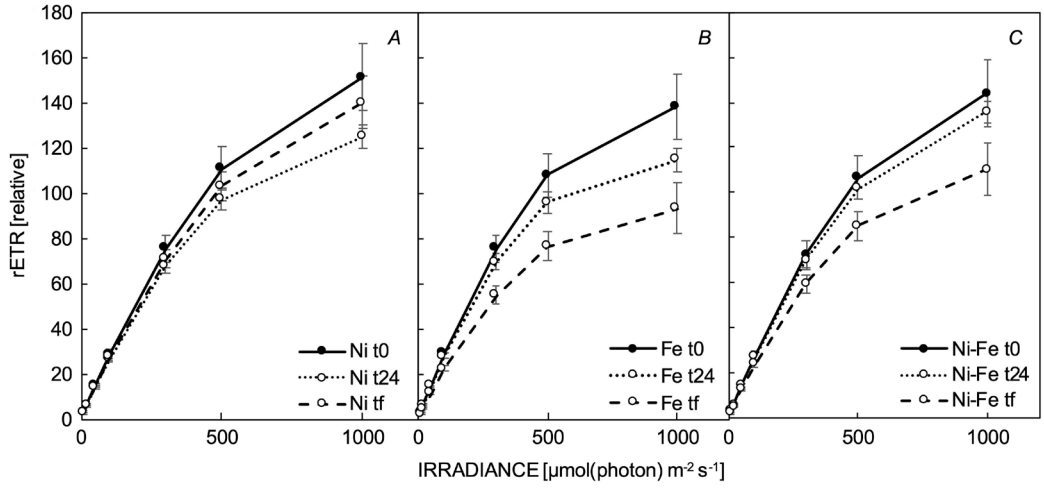

Fig. 4. Rapid light-response curves (RLCs) of *Heterocapsa* cf. *bohaiensis*, representing the relative electron transport rate (rETR) under increasing light intensities up to 1,000 µmol(photon) m^{-2} s^{-1} following Ni^{2+} (*A*), Fe^{2+} (*B*) or Ni^{2+}+Fe^{2+} (*C*) exposure at high concentrations at t_0, t_{24}, and t_f of the experiment.

Table 1. Rapid light curve parameters of *Heterocapsa* cf. *bohaiensis* in the presence of Ni^{2+}, Fe^{2+}, or Ni^{2+}+Fe^{2+} high concentrations at t_0, t_{24}, and t_f of the experiment. Values are expressed as mean area/cell ± SE (n = 3). Values are significantly different when p<0.05. rETRm – maximum relative electron transport rate; α – initial RLC slope; Ek – light-saturating index = ETRm/α; $NPQ_{induced}$ – nonphotochemical quenching induced by the RLC.

Metals		rETRm	α	Ek [µmol(photon) m^{-2} s^{-1}]	$NPQ_{induced}$
Ni^{2+}	t_0	181.67 ± 20.91	0.33 ± 0.02	546.82 ± 33.15	0.34 ± 0.09
	t_{24}	141.42 ± 5.39	0.31 ± 0.02	452.23 ± 24.71	0.29 ± 0.04
	t_f	166.30 ± 17.48	0.31 ± 0.01	529.02 ± 34.61	0.42 ± 0.06
Fe^{2+}	t_0	156.03 ± 11.26	0.35 ± 0.01	446.83 ± 18.42	0.30 ± 0.00
	t_{24}	123.88 ± 3.16	0.34 ± 0.01	361.43 ± 14.10	0.32 ± 0.05
	t_f	102.00 ± 17.99	0.27 ± 0.01	378.29 ± 48.06	0.39 ± 0.09
Ni^{2+}+Fe^{2+}	t_0	171.69 ± 8.10	0.32 ± 0.02	538.88 ± 31.15	0.42 ± 0.07
	t_{24}	169.22 ± 19.89	0.32 ± 0.01	532.66 ± 54.97	0.44 ± 0.11
	t_f	125.10 ± 10.85	0.28 ± 0.00	452.62 ± 34.84	0.42 ± 0.05
Kruskal–Wallis or Multifactor *ANOVA*					
A: Metal p(α=0.05)		<0.01	>0.05	<0.001 (F=37.58)	<0.05
B: Time p(α=0.05)		<0.001	<0.001	<0.001 (F=15.36)	>0.05
Interactions A × B		-	-	<0.005	-

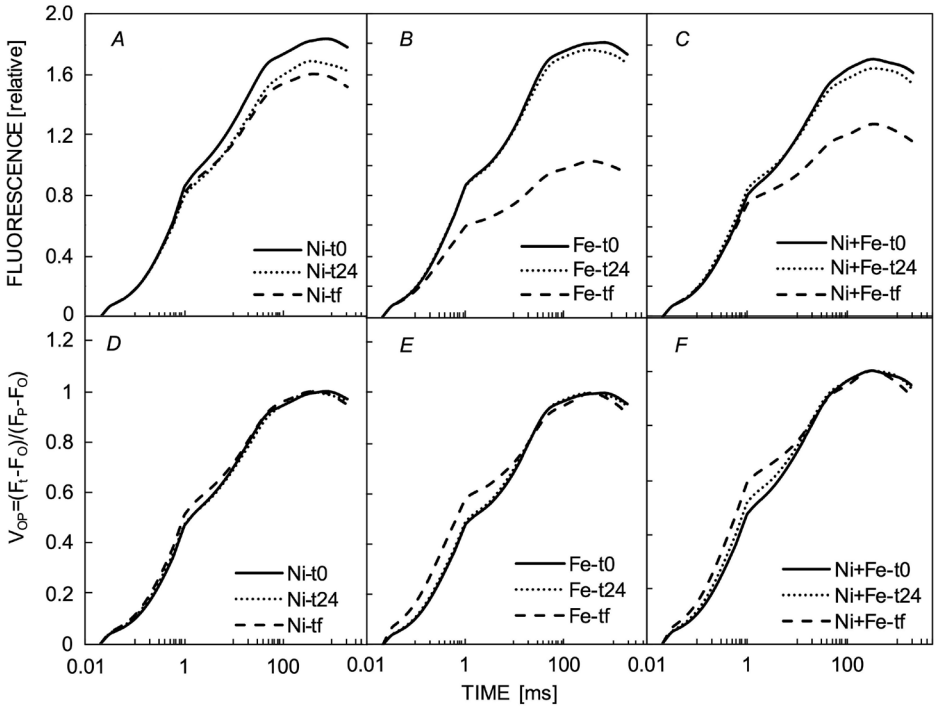

Fig. 5. Changes of Chl *a* fluorescence of *Heterocapsa* cf. *bohaiensis* after normalization at F_0 (*A–C*) and after double normalization at F_O to F_P phase (*D–F*) in the presence of Ni^{2+}, Fe^{2+}, or Ni^{2+}+Fe^{2+} at t_0, t_{24}, and t_f of the experiment.

attributed to the rate of Q_A reduction in the photosynthetic chain (Antal *et al.* 2009), was significantly higher after 13 d of Fe^{2+} and Ni^{2+}+Fe^{2+} (p<0.001 for both) exposure (Fig. 6). Similarly, the energy dissipation per reaction centre, DI_0/RC (p<0.01 for both), the trapped TR_0/RC (p<0.01 for both), and absorption of photons per reaction centre, ABS/RC (p<0.01 for both) were significantly higher after 13 d of Fe^{2+} and Ni^{2+}+Fe^{2+} high exposure (Fig. 6). However, the electron transfer per reaction centre, ET_0/RC, did not change significantly in response to metals (Fig. 6). For each varying parameter, the variations intensified in the following manner: Ni^{2+} < Ni^{2+}+Fe^{2+} < Fe^{2+}.

Discussion

The phylogenetic analysis clearly showed that both strains analysed belong to the genus *Heterocapsa*. The strain 19PV99 clustered in a group of sequences including strains

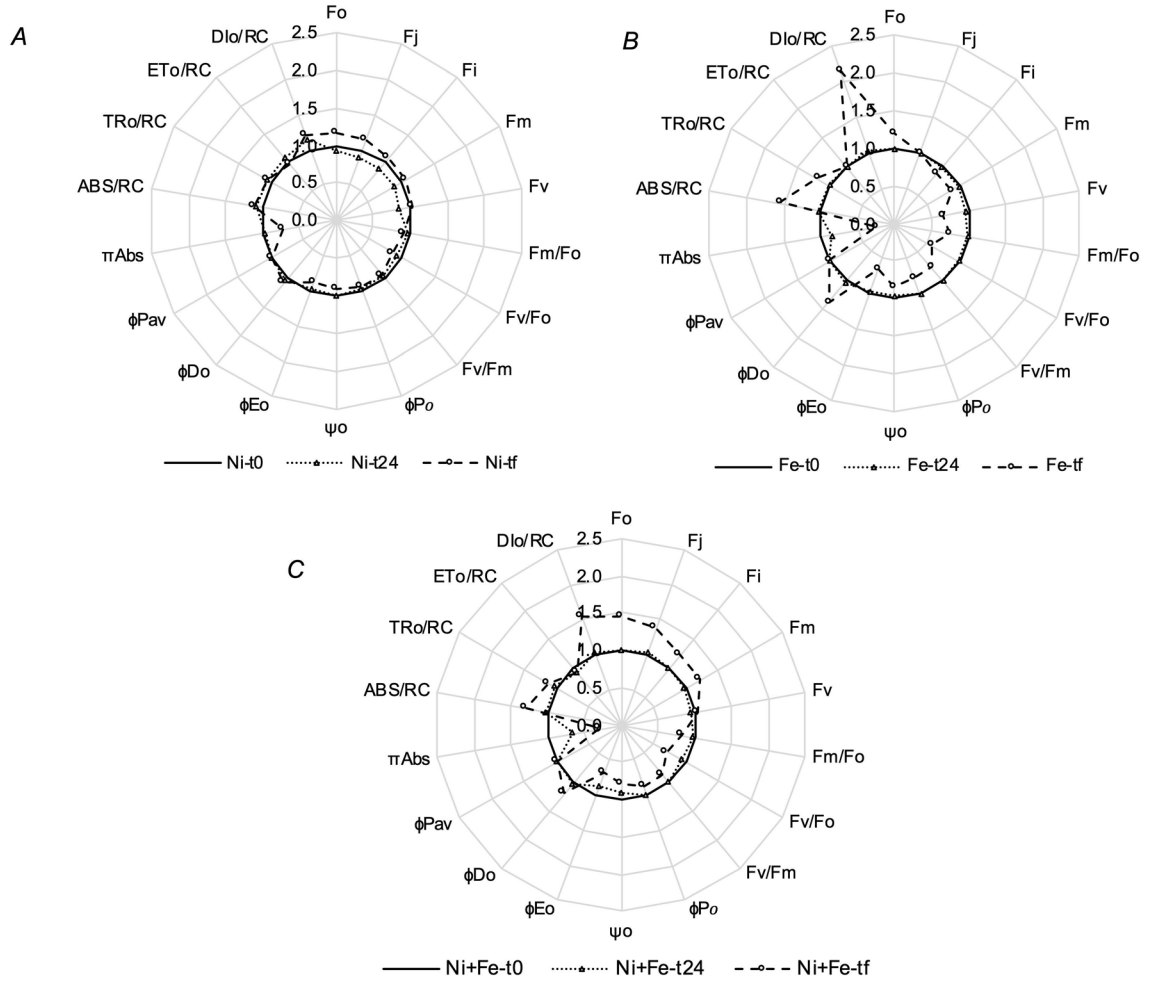

Fig. 6. Radar plot of fluorescence transient chlorophyll *a* parameters calculated from the JIP-test analysis of *Heterocapsa* cf. *bohaiensis* in the presence of Ni^{2+} (*A*), Fe^{2+} (*B*), or Ni^{2+}+Fe^{2+} (*C*) high concentrations at t_0, t_{24}, and t_f of the experiment. Normalised by the t_0 of each condition.

ascribed with different names but recently interpreted as *H. pygmaea* clade (Choi and Kim 2021). Whereas the strain 20PV100, the one exposed to the different trace metals, appeared closely related to *H. bohaiensis*, as indicated by phylogenetic position and *p*-distances calculated on the ITS region. The sequence of 20PV100 was not identical with sequences of *H. bohaiensis* from the type locality, but the level of divergence was low (around 2.0–2.5%). Compared with the threshold of 4% tentatively proposed by Litaker *et al.* (2007) to separate dinoflagellate species, strain 20PV100 can be considered as *H.* cf. *bohaiensis*, as detailed morphological features including morphology of thecal scales would be necessary to confirm the identity of the strain.

Heterocapsa cf. *bohaiensis* lives in New Caledonia coastal waters that are characterised by high Ni^{2+} and Fe^{2+} concentrations. In the present study, the addition of 58 mg(Ni^{2+}) L^{-1} did not affect *H.* cf. *bohaiensis* cell concentration. However, other species are more stressed by Ni^{2+} concentration. For example, cell concentration of the diatom *Phaeodactylum tricornutum* decreased when exposed to 1 mg(Ni^{2+}) L^{-1} (Guo *et al.* 2022), and the chlorophyte *Ankistodesmus falcatus* (Martínez-Ruiz and Martínez-Jerónimo 2015) was found to be stressed by 10^{-3} mg(Ni^{2+}) L^{-1}. This suggests that *H.* cf. *bohaiensis* is highly tolerant to Ni^{2+}. Conversely, the addition of Fe^{2+} at 55 mg L^{-1} induced a continuous drop in cell concentration throughout the 13 d of exposure. These results show that 55 mg L^{-1} of Fe^{2+} affects *H.* cf. *bohaiensis* growth. Growth retardation under Fe^{2+} high concentration has previously been reported in plants such as sweet potato (Chatterjee *et al.* 2006). In the microalgae *Chlorella sorokiniana*, the Fe^{2+} growth retardation threshold appears at 250 mg L^{-1} (Wan *et al.* 2014) suggesting that *H.* cf. *bohaiensis* is not particularly tolerant to high Fe^{2+} concentrations. However, the absence of photoinhibition indicated by the absence of rETR decline at high irradiance in the RLCs suggests that the stress induced by this metal is moderated, meaning that no toxic light stress was induced by the tested PAR under the different metal exposures.

To evaluate *H.* cf. *bohaiensis* fitness under metal stresses, photosynthesis performance was assessed by

chlorophyll *a* fluorescence measurements using PAM fluorometry (Kumar *et al.* 2014). Nickel addition did not affect photosynthetic parameters further supporting that this species is highly tolerant to high Ni^{2+} concentrations. *H.* cf. *bohaiensis* may be adapted to the Ni^{2+} high concentrations present in New Caledonia coastal waters. Interestingly, in the presence of 55 mg(Fe^{2+}) L^{-1}, photosynthesis efficiency decreased as shown by the maximal light-utilization efficiency of PSII reduction (F_v/F_m). The typical F_v/F_m values for dinoflagellates are between 0.6 and 0.7 (Napoléon *et al.* 2013, Cooney *et al.* 2019). A similar but lower decrease in photosynthetic efficiency was observed in the algae exposed to the metal mixture at 29 mg(Ni^{2+}) L^{-1} and 28 mg(Fe^{2+}) L^{-1} suggesting that Ni^{2+} high concentrations do not participate in the Fe^{2+}-induced loss of photosynthesis efficiency and the toxic mechanisms can thus be attributed to Fe^{2+} ions only.

Rapid light curve parameters assessed the ability of *H.* cf. *bohaiensis* to utilize light energy from 0 to 1,000 µmol(photon) m^{-2} s^{-1}. The RLCs typically exhibit three distinct phases, a first increase corresponding to the light-limiting linear region, followed by a light-saturating plateau and photoinhibition (Ralph and Gademann 2005). Both proxies, α, a proxy of the ability to utilize low light intensities, and Ek representing the ability to utilize high light intensities decreased in Fe^{2+} and Ni^{2+}+Fe^{2+} conditions. It suggests that *H.* cf. *bohaiensis* ability to use light is reduced by Fe^{2+} ions at high concentrations in our experiment. The relative electron transport rate (rETR) and the maximum relative electron transport rate (rETRm) decreased in the presence of Fe^{2+} in excess suggesting a disruption in the electron transport chain. The electron transport in the thylakoid membrane relies on the successive reduction of Q_A, Q_B, plastoquinone (PQ), plastocyanin (PC), ferredoxin (Fd), and finally NADP. The JIP-test allows us to characterize the efficiency of light absorption occurring in the PSII and the subsequent electron transport at specific electron acceptors of the transport chain by (*1*) quantum yield and (*2*) specific fluxes indicators (Strasser and Strasser 1995). The parameters that describe the specific fluxes of absorption (ABS/RC) and trapping (TR_0/RC) of light energy at the PSII intensifies indicating that these fluxes became more efficient under high Fe^{2+} exposure. This suggests that Fe^{2+} high concentrations might stimulate the capture and absorption of light energy at the PSII. This effect has also been described in sweet potatoes in response to excess Fe^{2+} (Adamski *et al.* 2011). In higher plants (*e.g.*, sweet potato), excess Fe^{2+} also intensifies the subsequent electron transport rate until PQ reduction after which the electron transport rate remains unchanged (Adamski *et al.* 2011). Interestingly, in our study, the parameters that describe the electron transport rate quantum efficiency decreased. Especially ψ_0, the probability that an exciton goes further than Q_A in the electron transport chain, and φE_0, the quantum yield of electron transport, decreased indicating that the electron transport rate slowed down from the Q_A to Q_B electron transmission. Similarly, the performance index πAbs that describes the probability that an electron goes from PSII to the PQ pool decreased. Finally, the shape of the OJIP transient indicated that the electron transport rate to PSI decreased. All together, these results suggest that light absorption and Q_A reduction is enhanced by an excess in Fe^{2+} ions but the electron transport is inhibited from Q_B until PSI. The electron transport rate reduction can occur due to (*1*) a simultaneous decrease at each reduction step of the chain (*e.g.*, Q_A to Q_B to PQ to PC to Fd *via* PSI and finally NAPD) or (*2*) a decrease at the first decreased step (Q_A to Q_B) that slows down the kinetic of the following reducing steps.

In the cell, Fe is the more ubiquitous metal directly bound to proteins (metal cofactors) and involved in the electron transport chain (Yruela 2013). This is attributed to the high redox power of the Fe^{2+}/Fe^{3+} couple. Fe^{2+} participates in PSII, cytochrome b_6f (Cyt b_6f), PSI, and ferredoxin structures that each catalyse the transfer of electrons from one acceptor to the next one (Yruela 2013). Indeed, Fe is present in Fe-S clusters and heme that compose cytochrome b_{559} (Cyt b_{559}) of PSII, Cyt b_6f complex, PSI, and ferredoxin (Yruela 2013). In the PSII, Fe^{2+} ions compose the nonheme iron-binding site of Q_A and Q_B (Müh *et al.* 2012). The deficiency in Fe is well documented in plants and microalgae and is responsible for the electron transport rate decrease (Msilini *et al.* 2011). On the contrary, Fe toxicity mechanisms remain poorly described. Photosynthetic decrease and growth retardations in response to Fe excess are mainly attributed to reactive oxygen species (ROS) production increase and the following lipids and proteins oxidation (Pinto *et al.* 2016, Danouche *et al.* 2022). Indeed free Fe^{2+} ions participate in the formation of hydroxyl radical •HO and reactive oxygen RO through redox cycles (Ravet and Pilon 2013). These reactions require O_2 and H_2O_2 which are abundant in the chloroplast due to the oxygenic photochemical reactions (Ravet and Pilon 2013). Therefore, the increase in Fe^{2+} free ions enhances •HO and RO productions in chloroplasts (Ravet and Pilon 2013). •HO and RO's main action in cells is the lipid peroxidation of membranes. Therefore, it is possible that in presence of Fe in excess, an accumulation of •HO and RO destabilized the thylakoid membrane disrupting the electron transfer. Furthermore, Fe-S containing enzymes are inhibited when oxidized by O_2 (Danouche *et al.* 2022). Therefore, Cyt b_6f, PSI, and ferredoxin electron transfer catalysers may be particularly sensitive to Fe^{2+}-induced ROS.

Nonphotochemical quenching, a photoprotective mechanism that dissipates excessive light into heat did not show variation under high Fe^{2+} exposure, while the specific flux of dissipation into heat (DI_0/RC) increased. This can be explained by the light intensities used to measure these parameters. NPQ induced was measured in response to 1,000 µmol(photon) m^{-2} s^{-1} during the last step of the RLC, while DI_0/RC was measured under a 2-s saturating light pulse at 3,000 µmol(photon) m^{-2} s^{-1} during the OJIP experiment. These results suggest that light intensity around 1,000 µmol(photon) m^{-2} s^{-1} is not inhibitory to PSII.

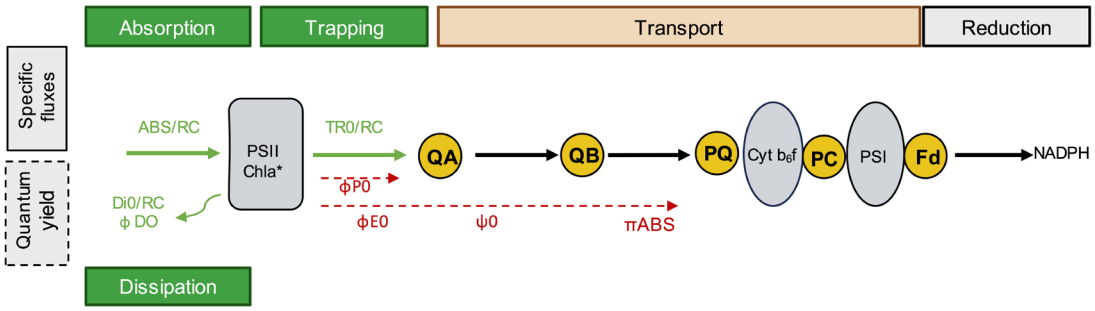

Fig. 7. Resume of JIP parameters describing specific fluxes (*plain arrows*) and quantum yield (*dashed arrows*) of energy transfer in the photosynthetic chain in presence of Fe^{2+}. *Green arrows* show an increase and *red arrows* a decrease of the specific fluxes and yields observed with *Heterocapsa* cf. *bohaiensis* exposed to Fe^{2+} high concentration.

Conclusion: We showed that *H.* cf. *bohaiensis* was highly tolerant to Ni^{2+} but sensitive to Fe^{2+} concentrations reported to be toxic to other microalgae species. The Fe^{2+} stress induced a reduction of the photosynthesis efficiency that might be due to a disruption in the electron transport chain starting at the Q_B reducing step rather than a defect in light absorption and trapping of the PSII (Fig. 7). This can be explained by a higher ROS production that destabilizes the electron transport catalysers in the thylakoid membrane. The Fe^{2+} stress also induced an increase of absorption, trapping, and dissipation of specific fluxes (Fig. 7). These results are a first step forward in the understanding of adaptation of dinoflagellate to the high metal concentration specific context and brought additional insights into the toxic mechanisms of Fe in microalgae.

References

Adamski J.M., Peters J.A., Danieloski R., Bacarin M.A.: Excess iron-induced changes in the photosynthetic characteristics of sweet potato. – J. Plant Physiol. **168**: 2056-2062, 2011.

Ambatsian P., Fernex F., Bernat M. *et al.*: High metal inputs to closed seas: the New Caledonian lagoon. – J. Geochem. Explor. **59**: 59-74, 1997.

Antal T.K., Matorin D.N., Ilyash L.V. *et al.*: Probing of photosynthetic reactions in four phytoplanktonic algae with a PEA fluorometer. – Photosynth. Res. **102**: 67-76, 2009.

Bird E.C.F., Dubois J.-P., Iltis J.A.: The Impacts of Opencast Mining on the Rivers and Coasts of New Caledonia. Pp. 53. United Nations University, Tokyo 1984.

Biscéré T., Lorrain A., Rodolfo-Metalpa R. *et al.*: Nickel and ocean warming affect scleractinian coral growth. – Mar. Pollut. Bull. **120**: 250-258, 2017.

Biscéré T., Rodolfo-Metalpa R., Lorrain A. *et al.*: Responses of two scleractinian corals to cobalt pollution and ocean acidification. – PLoS ONE **10**: e0122898, 2015.

Boisvert S., Joly D., Leclerc S. *et al.*: Inhibition of the oxygen-evolving complex of photosystem II and depletion of extrinsic polypeptides by nickel. – BioMetals **20**: 879-889, 2007.

Chatterjee C., Gopal R., Dube B.K.: Impact of iron stress on biomass, yield, metabolism and quality of potato (*Solanum tuberosum* L.). – Sci. Hortic.-Amsterdam **108**: 1-6, 2006.

Chénais B.: Algae and microalgae and their bioactive molecules for human health. – Molecules **26**: 1185, 2021.

Choi H., Kim S.: *Heterocapsa busanensis* sp. nov. (Peridiniales, Dinophyceae): A new marine thecate dinoflagellate from Korean coastal waters. – Eur. J. Protistol. **79**: 125797, 2021.

Consalvey M., Perkins R.G., Paterson D.M., Underwood G.J.C.: PAM fluorescence: a beginners guide for benthic diatomists. – Diatom Res. **20**: 1-22, 2005.

Cooney E.C., Fredrickson K.A., Bright K.J., Strom S.L.: Contrasting effects of high-intensity photosynthetically active radiation on two bloom-forming dinoflagellates. – J. Phycol. **55**: 1082-1095, 2019.

Coulombier N., Blanchier P., Le Dean L. *et al.*: The effects of CO_2-induced acidification on *Tetraselmis* biomass production, photophysiology and antioxidant activity: A comparison using batch and continuous culture. – J. Biotechnol. **325**: 312-324, 2021.

Coulombier N., Nicolau E., Le Déan L. *et al.*: Impact of light intensity on antioxidant activity of tropical microalgae. – Mar. Drugs **18**: 122, 2020.

Dahmen-Ben Moussa I., Athmouni K., Chtourou H. *et al.*: Phycoremediation potential, physiological, and biochemical response of *Amphora subtropica* and *Dunaliella* sp. to nickel pollution. – J. Appl. Phycol. **30**: 931-941, 2018.

Danouche M., El Ghatchouli N., Arroussi H.: Overview of the management of heavy metals toxicity by microalgae. – J. Appl. Phycol. **34**: 475-488, 2022.

Darriba D., Taboada G.L., Doallo R., Posada D.: jModelTest 2: more models, new heuristics and parallel computing. – Nat. Methods **9**: 772, 2012.

Fox J.M., Zimba P.V.: Minerals and trace elements in microalgae. – In: Levine I.A., Fleurence J. (ed.): Microalgae in Health and Disease Prevention. Pp. 177-193. Academic Press, London 2018.

Freeman M.A., Yokoyama H., Ogawa K.: A microsporidian parasite of the genus *Spraguea* in the nervous tissues of the Japanese anglerfish *Lophius litulon*. – Folia Parasit. **51**: 167-176, 2004.

Gouy M., Guindon S., Gascuel O.: SeaView version 4: A multi-platform graphical user interface for sequence alignment and phylogenetic tree building. – Mol. Biol. Evol. **27**: 221-224, 2010.

Guillard R.R.L., Hargraves P.E.: *Stichochrysis immobilis* is a diatom, not a chrysophyte. – Phycologia **32**: 234-236, 1993.

Guindon S., Dufayard J.-F., Lefort V. *et al.*: New algorithms and methods to estimate maximum-likelihood phylogenies: assessing the performance of PhyML 3.0. – Syst. Biol. **59**: 307-321, 2010.

Guo R., Lu D., Liu C. *et al.*: Toxic effect of nickel on microalgae *Phaeodactylum tricornutum* (Bacillariophyceae). – Ecotoxicology **31**: 746-760, 2022.

Hédouin L., Metian M., Lacoue-Labarthe T. *et al.*: Influence of

food on the assimilation of selected metals in tropical bivalves from the New Caledonia lagoon: qualitative and quantitative aspects. – Mar. Pollut. Bull. **61**: 568-575, 2010.

Katoh K., Rozewicki J., Yamada K.D.: MAFFT online service: multiple sequence alignment, interactive sequence choice and visualization. – Brief. Bioinform. **20**: 1160-1166, 2019.

Kumar K.S., Dahms H.-U., Lee J.-S. *et al.*: Algal photosynthetic responses to toxic metals and herbicides assessed by chlorophyll *a* fluorescence. – Ecotox. Environ. Safe. **104**: 51-71, 2014.

Le Grand H., Moreton B., Dolbecq M. *et al.*: Suivi environnemental colonne d'eau 2010–2012. [Water column environmental monitoring 2010–2012.] OEIL, 2013. [In French] *Available at*: https://oeil.nc/cdrn/index.php/resource/bibliographie/view/5724.

Leong Y.K., Chang J.-S.: Bioremediation of heavy metals using microalgae: Recent advances and mechanisms. – Bioresource Technol. **303**: 122886, 2020.

Litaker R.W., Vandersea M.W., Kibler S.R. *et al.*: Recognizing dinoflagellate species using its rDNA sequences. – J. Phycol. **43**: 344-355, 2007.

Mandal M.K., Saikia P., Chanu N.K., Chaurasia N.: Modulation of lipid content and lipid profile by supplementation of iron, zinc, and molybdenum in indigenous microalgae. – Environ. Sci. Pollut. Res. **26**: 20815-20828, 2019.

Martínez-Ruiz E.B., Martínez-Jerónimo F.: Nickel has biochemical, physiological, and structural effects on the green microalga *Ankistrodesmus falcatus*: An integrative study. – Aquat. Toxicol. **169**: 27-36, 2015.

Menguy E., Dumontet V., Coulombier N. *et al.*: A method to assess algicidal activity of microalgal extracts coupling microalgae produced in stirred closed photobioreactor operating in continuous with pulse amplitude modulated (PAM) fluorometry. – MethodsX **7**: 101037, 2020.

Merrot P.: Géochimie spéciation et mobilité des éléments traces métalliques (Fe, Ni, Cr et Mn) au sein des sédiments du lagon de Nouvelle-Calédonie. [Geochemical speciation and mobility of trace metals (Fe, Ni, Cr and Mn) in New Caledonian lagoon sediments.] PhD Thesis. Pp. 345. Sorbonne Université, 2019. [In French]

Merrot P., Juillot F., Flipo L. *et al.*: Bioavailability of chromium, nickel, iron and manganese in relation to their speciation in coastal sediments downstream of ultramafic catchments: A case study in New Caledonia. – Chemosphere **302**: 134643, 2022.

Mimouni V., Ulmann L., Pasquet V. *et al.*: The potential of microalgae for the production of bioactive molecules of pharmaceutical interest. – Curr. Pharm. Biotechnol. **13**: 2733-2750, 2012.

Msilini N., Zaghdoudi M., Govindachary S. *et al.*: Inhibition of photosynthetic oxygen evolution and electron transfer from the quinone acceptor Q_A^- to Q_B by iron deficiency. – Photosynth. Res. **107**: 247-256, 2011.

Müh F., Glöckner C., Hellmich J., Zouni A.: Light-induced quinone reduction in photosystem II. – BBA-Bioenergetics **1817**: 44-65, 2012.

Napoléon C., Raimbault V., Claquin P.: Influence of nutrient stress on the relationships between PAM measurements and carbon incorporation in four phytoplankton species. – PLoS ONE **8**: e66423, 2013.

Nunn G.B., Theisen B.F., Christensen B., Arctander P.: Simplicity-correlated size growth of the nuclear 28S ribosomal RNA D3 expansion segment in the crustacean order Isopoda. – J. Mol. Evol. **42**: 211-223, 1996.

Pelletier B.: Geology of the New Caledonia region and its implications for the study of the New Caledonian biodiversity. – In: Payri C.E., Richer de Forges B. (ed.): Compendium of Marine Species of New Caledonia. Pp. 19-32. IRD, Nouméa 2007.

Pinto S.D.S., Souza A.E.D., Oliva M.A., Pereira E.G.: Oxidative damage and photosynthetic impairment in tropical rice cultivars upon exposure to excess iron. – Sci. Agric. **73**: 217-226, 2016.

Platt T., Gallegos C.L., Harrison W.G.: Photoinhibition of photosynthesis in natural assemblages of marine phytoplankton. – J. Mar. Res. **38**: 687-701, 1980.

Quigg A.: Micronutrients. – In: Borowitzka M.A., Beardall J., Raven J.A. (ed.): The Physiology of Microalgae. Developments in Applied Phycology. Vol. 6. Pp. 211-231. Springer, Cham 2016.

Ralph P.J., Gademann R.: Rapid light curves: a powerful tool to assess photosynthetic activity. – Aquat. Bot. **82**: 222-237, 2005.

Ravet K., Pilon M.: Copper and iron homeostasis in plants: the challenges of oxidative stress. – Antioxid. Redox Sign. **19**: 919-932, 2013.

R Core Team: R: A language and environment for statistical computing, 2017. *Available at*: https://www.r-project.org/.

Ronquist F., Huelsenbeck J.P.: MrBayes 3: Bayesian phylogenetic inference under mixed models. – Bioinformatics **19**: 1572-1574, 2003.

Sathasivam R., Ki J.-S.: A review of the biological activities of microalgal carotenoids and their potential use in healthcare and cosmetic industries. – Mar. Drugs **16**: 26, 2018.

Satoh A., Vudikaria L.Q., Kurano N., Miyachi S.: Evaluation of the sensitivity of marine microalgal strains to the heavy metals, Cu, As, Sb, Pb and Cd. – Environ. Int. **31**: 713-722, 2005.

Scholin C.A., Herzog M., Sogin M., Anderson D.M.: Identification of group- and strain-specific genetic markers for globally distributed *Alexandrium* (Dinophyceae). II. Sequence analysis of a fragment of the LSU rRNA gene. – J. Phycol. **30**: 999-1011, 1994.

Schreiber U., Bilger W., Neubauer C.: Chlorophyll fluorescence as a nonintrusive indicator for rapid assessment of *in vivo* photosynthesis. – In: Schulze E.-D., Caldwell M.M. (ed.): Ecophysiology of Photosynthesis. Pp. 49-70. Springer, Berlin-Heidelberg 1995.

Seco J., Aparício S., Brierley A.S. *et al.*: Mercury biomagnification in a Southern Ocean food web. – Environ. Pollut. **275**: 116620, 2021.

Strasser B.J., Strasser R.J.: Measuring fast fluorescence transients to address environmental questions: The JIP test. – In: Mathis P. (ed.): Photosynthesis: From Light to Biosphere. Vol. 5. Pp. 977-980. Kluwer Academic Publishers, Dordrecht 1995.

Tamura K., Stecher G., Kumar S.: MEGA11: Molecular evolutionary genetics analysis version 11. – Mol. Biol. Evol. **38**: 3022-3027, 2021.

Wan M., Jin X., Xia J. *et al.*: The effect of iron on growth, lipid accumulation, and gene expression profile of the freshwater microalga *Chlorella sorokiniana*. – Appl. Microbiol. Biot. **98**: 9473-9481, 2014.

Wang H., Su Q., Zhuang Y. *et al.*: Effects of iron valence on the growth, photosynthesis, and fatty acid composition of *Phaeodactylum tricornutum*. – J. Mar. Sci. Eng. **11**: 316, 2023.

Xiao J., Sun N., Zhang Y. *et al.*: *Heterocapsa bohaiensis* sp. nov. (Peridiniales: Dinophyceae): a novel marine dinoflagellate from the Liaodong Bay of Bohai Sea, China. – Acta Oceanol. Sin. **37**: 18-27, 2018.

Yong W.-K., Sim K.-S., Poong S.-W. *et al.*: Physiological and metabolic responses of *Scenedesmus quadricauda*

(Chlorophyceae) to nickel toxicity and warming. – 3 Biotech **9**: 315, 2019.

Yruela I.: Transition metals in plant photosynthesis. – Metallomics **5**: 1090-1109, 2013.

Zhang Y., Feng T., Qu J. *et al.*: Toxicity and haemolytic activity of a newly described dinoflagellate, *Heterocapsa bohainensis* to the rotifer *Brachionus plicatilis*. – Harmful Algae **84**: 112-118, 2019.